JOURNAL OF GUIDANCE, CONTROL, AND DYNAMICS
Vol. 24, No. 2, March–April 2001

Numerical Investigation of Model Reference Adaptive Control for Hypersonic Aircraft

E. Mooij*
Delft University of Technology, 2600 GB Delft, The Netherlands

To address the attitude control of hypersonic aircraft, an approach of direct model reference adaptive control (MRAC) is followed. The basis for MRAC is that a system of which only the outputs are known has to track a reference model that can be a simple approximation of the actual system. By combining the output error, the model state, and the model control parameters into a reference signal, proportional and integral gains can be computed that are adapted to the value of the reference signal. To apply MRAC it is necessary that the controlled nonlinear system is almost strictly passive. The design of the combined longitudinal/lateral MRAC system is centred around a linearized reference model of the winged cone configuration at a Mach 5.6 fight condition. The results of some fundamental response tests are discussed, as well as altitude and cross-range transitions. It appears that MRAC seems to be a promising concept when applied to hypersonic space planes. Although it is too early to say that the current configuration of the controller is robust with respect to design uncertainties and environmental perturbations, there are still many improvements possible that will enhance performance. One drawback, however, is the large number of design parameters that can be tuned to influence the performance.

Nomenclature

$\boldsymbol{A}$	=	state or system matrix
$\boldsymbol{B}$	=	control input matrix
b_{ref}	=	aerodynamic reference length, m
$\boldsymbol{C}$	=	output matrix
C_D, C_S, C_L	=	drag, side-force, and lift coefficients
C_l, C_m, C_n	=	roll-, pitch-, and yaw-moment coefficients
c_{ref}	=	aerodynamic reference length, m
$\boldsymbol{e}_y$	=	output error, rad
h	=	height, m
I	=	moment (product) of inertia, kg · m^2
$\boldsymbol{J}$	=	cost criterion
K	=	control gain, 1/rad
$\boldsymbol{K}$	=	control-gain matrix
L	=	roll moment, Nm
L_e	=	equilibrium lift, N
M	=	Mach number
N	=	yaw moment, Nm
p, q, r	=	roll, pitch, and yaw rates, rad/s
$\boldsymbol{Q}$	=	control deviation weight matrix
$\boldsymbol{R}$	=	control effort weight matrix
$\boldsymbol{r}$	=	model reference adaptive control concatenated state vector
S_{ref}	=	aerodynamic reference area, m^2
$\boldsymbol{T}_p, \boldsymbol{T}_i$	=	weighting matrix proportional, integral gain
t	=	time, s
$\boldsymbol{u}$	=	control vector
$\boldsymbol{x}$	=	state vector
y	=	cross range, m
$\boldsymbol{y}$	=	output vector
α	=	angle of attack, rad
β	=	angle of sideslip, rad
γ	=	flight-path angle, rad
$\Delta..$	=	perturbation
δ	=	geocentric latitude, rad
δ_a	=	aileron deflection angle, rad
δ_e	=	elevator/elevon deflection angle, rad
δ_r	=	rudder deflection angle, rad
δ_T	=	throttle setting
ζ	=	damping ratio
σ	=	bank angle, rad
σ_i	=	integral-gain coefficient
τ	=	geocentric longitude, rad
χ	=	heading, rad
ω	=	eigenfrequency, rad/s

Indices

c	=	commanded
e	=	equilibrium
i	=	integral
m	=	model
p	=	plant; proportional
0	=	initial condition

Received 26 April 1999; revision received 6 June 2000; accepted for publication 5 July 2000.

*Ph.D. Candidate, P.O. Box 5058, Faculty of Aerospace Engineering; currently Lead Engineer, Fokker Space B.V., P.O. Box 32070, 2303 DB Leiden, The Netherlands; e.mooij@fokkerspace.nl. Member AIAA.

I. Introduction

HORIZONTAL takeoff single- and two-stage-to-orbit vehicles using air-breathing propulsion, also known as aerospace planes, seem to be promising concepts for more economical delivery of payloads to orbit. The effective use of air-breathing propulsion engines leads to ascent trajectories at lower altitudes as compared to conventional launchers, resulting in higher dynamic pressures, higher skin-surface temperatures, and higher acceleration loads. Apart from innovating fields such as heat-resistant materials and structures, the development of guidance logic and attitude controllers poses a challenging problem, in particular due to the small performance margin and the strongly varying flight environment.

Experience with the space shuttle shows that the vehicle's pressure distribution is strongly dependent on angle of attack and Mach number, as well as real-gas effects at Mach numbers in excess of 10 (Ref. 1). Because of the shifting center of pressure at high Mach numbers, longitudinal stability problems may occur due to the resulting destabilizing nose-up moment. However, for a proper performance of the propulsion system, an accurate angle-of-attack control is required because large variations in thrust force and moment can result from minor angle-of-attack perturbations.[2] The picture is even more complicated because of the aeroelastic–propulsive interaction, a common problem for long, slender bodies. Turbulence-induced aeroelastic geometry perturbations were shown to produce significant longitudinal force and moment components.[3] Because the performance of a space plane is marginal at best, there may be a large number of airframe–engine dynamic deficiencies left to be corrected by control means, after a trimmed state for the point-mass performance has been established.[4]

However, inattention to the overall control issues may lead to an optimistic estimate of the performance, which can have a severe influence on design changes at a later stage. Control limitations on older aircraft have sometimes limited the available flight envelope.[5]

It may be obvious that attitude control of hypersonic space planes is a real challenge and should not be considered lightly. Classical proportional–derivative (PD) controllers with large (time-varying) gains may theoretically guarantee a good performance and fast stabilization, although large gains would imply, in general, high noise amplification and high cost of control. Moreover, it may be difficult to guarantee the required robustness for this type of vehicle. In the past few years, the use of H_∞ control and μ synthesis has gained interest as attitude controller of a space plane at Mach = 8. (Refs. 6 and 7). Despite the encouraging results, some drawbacks were also identified.[8,9] Because of the (very conservative) guarantees of robustness (H_∞), a large performance penalty can result. Compensators based on μ synthesis are much less conservative than H_∞ designs, but are computationally infeasible for large-order plants (the order of the control system increases drastically). Model-order reduction proved to be a delicate numerical problem.[6,9]

Yet another robust-control technique is that of adaptive control, when in some way the controller parameters are adapted to the changing circumstances. Adaptive control, a special type of nonlinear feedback control, found its way into use in the early 1950s, as an autopilot for high-performance aircraft, later on followed by applications in the F-94, F-101, and X-15 research aircraft.[10] Throughout the succeeding years, several different adaptive techniques were developed, of which three are more common: gain scheduling, self-tuning regulation, and model reference adaptive control (MRAC). The problem of self-adjusting the parameters of a controller to stabilize the dynamic characteristics of a feedback control system when drift variations in the plant parameters occur was the origin of MRAC.[11] With this technique, a reference model serves as the basis to generate the steering commands for the (unknown) plant. The parameters of the controller are adjusted in such a way that the difference between the model output and the plant output are minimized. The performance of the controller is in this way less sensitive to environmental changes, modeling errors, and nonlinearities within the system. A drawback might be, however, that a large control effort can be required to make the plant follow the model.[12]

A recent work on direct adaptive control algorithms, and especially a simplified form of MRAC, is found in Ref. 13. The approach aims at simple adaptive control based on output feedback, requiring neither full state feedback nor adaptive observers. It may be obvious that this is very appealing because it puts the fewest restrictions on the controller. Three important properties of this concept include the following:

1) It is applicable to nonminimum phase systems.

2) The order, that is, number of states, of the physical system may be much larger than the order of the reference model (note, the number of model outputs must be equal to the number of plant outputs).

3) It considers plants with multiple inputs and outputs, so-called multi-input/multi-output (MIMO) systems.

MRAC has been studied as a control application of large flexible space structures, that is, the space station.[14,15] The controller appeared to be robust, also under the severe conditions of shuttle docking and mass and inertia changes. Because the application of MRAC to hypersonic aircraft has not been widely studied yet, in this paper we will present a design of such a controller to identify its potential use for this kind of vehicles. The selected hypersonic aircraft reference model is the winged cone configuration (Sec. II), a vehicle concept developed by NASA. After an introduction to the mathematical foundation of MRAC (Sec. III), the actual design of the adaptive controller will be discussed in Sec. IV. In Sec. V, simulation results of some fundamental response tests and an altitude and cross-range transition at Mach = 5.6 are presented. Section VI, finally, will conclude this paper. The current paper summarizes the results presented in Ref. 16. There, the application of MRAC to the vertical-plane ascent to orbit is analyzed as well.

II. Hypersonic Aircraft Reference Model

The winged cone configuration (WCC) reference vehicle, also known as the Langley accelerator, is a generic, horizontal takeoff, single-stage-to-orbit configuration that can be used for point-mass as well as six-degrees-of-freedom simulations.[17] The WCC has a dry mass of 58,968 kg and consists of an axisymmetric 5-deg half-angle conical forebody, a cylindrical engine nacelle section, and a cone frustrum nozzle. The wing has a leading-edge sweep of 78 deg and is set at 0-deg incidence and dihedral. The wing is a 4% thick diamond airfoil, with the elevons located at the trailing edge of the wing (positive deflections are with the trailing edge down). The vertical tail is a 4% thick diamond airfoil with a leading-edge sweep angle of 70 deg and includes a rudder with a hinge line at the 75% chord position measured from the leading edge (positive deflections are with the trailing edge left). The takeoff mass of the vehicle is 136,079 kg. The aerodynamic properties of the vehicle have been modeled as tabulated functions of Mach number, angles of attack and sideslip, and control-surface deflection. The propulsion system comprises tables for the thrust and specific impulse as a function of Mach number and dynamic pressure. Linear interpolation is used in either case to obtain the actual values.

The guidance system for hypersonic maneuvres is based on a combination of altitude and cross-range control.[18] The corresponding commanded accelerations follow from two separate proportional–integral–derivative (PID) guidance laws, that is, one for altitude and one for cross range. Conversion of the commanded accelerations to a normal load (and, subsequently, an angle of attack) and bank angle are executed by a so-called resolver, thereby taking centrifugal relief into account. In case of conflicting commands, altitude control has priority over cross-range control. Finally, the throttle-control law is a PD regulator that tracks a maximum dynamic pressure. More details on this throttle-control law, as well on the applied simulation model can be found in Ref. 16.

III. MRAC

The space plane considered in this study is only a simple representation of a realistic space plane. Basically, long slender bodies suffer from aeroelastic effects that can influence the performance significantly. Although aeroelasticity is not covered, the motion of the remaining nonelastic, mass-varying body with respect to a rotating, oblate Earth is described by a set of complex, nonlinear differential equations[16]:

$$\dot{\boldsymbol{x}}_p = \boldsymbol{f}[t, \boldsymbol{x}_p(t), \boldsymbol{u}_p(t)] \tag{1a}$$

$$\boldsymbol{y}_p = \boldsymbol{g}[\boldsymbol{x}_p(t), \boldsymbol{u}_p(t)] \tag{1b}$$

where $\boldsymbol{x}_p(t)$ is the $n_p \times 1$ plant state vector, $\boldsymbol{u}_p(t)$ is the $m \times 1$ plant input or command vector, $\boldsymbol{y}_p(t)$ is the $q \times 1$ model output vector, and $\boldsymbol{f}$ and $\boldsymbol{g}$ are $n_p \times 1$ and $q \times 1$ vector functions.

For the development of a control system, it is common practice to linearize the preceding nonlinear model. However, when such a controller is applied to the original system, some kind of performance feedback should be included to account for the nonlinearities. In the subsequent discussion, the following linearized model of the space plane will be used:

$$\dot{\boldsymbol{x}}_m(t) = \boldsymbol{A}_m \boldsymbol{x}_m(t) + \boldsymbol{B}_m \boldsymbol{u}_m(t) \tag{2a}$$

$$\boldsymbol{y}_m(t) = \boldsymbol{C}_m \boldsymbol{x}_m(t) \tag{2b}$$

where $\boldsymbol{x}_m(t)$ is the $n_m \times 1$ model state vector; $\boldsymbol{u}_m(t)$ is the $m \times 1$ model input or command; $\boldsymbol{y}_m(t)$ is the $q \times 1$ model output vector; and $\boldsymbol{A}_m$, $\boldsymbol{B}_m$, and $\boldsymbol{C}_m$ are the state, control, and output matrices of appropriate dimensions.

MRAC is based on matching the response of the system that is to be controlled (the plant) to that of a reference model (the model). In its simplest form, an MRAC system requires the model input $\boldsymbol{u}_m$ and model state $\boldsymbol{x}_m$ to form part of the input signal $\boldsymbol{u}_p$ to the plant (note that the number of model inputs and outputs equals the

corresponding number of plant inputs and outputs). Moreover, the so-called output error $\boldsymbol{e}_y$ serves as a feedback quantity to form the third element that composes $\boldsymbol{u}_p$, such that the adaptive system uses all values that can be measured. The three gains, that is, $\boldsymbol{K}_x$, $\boldsymbol{K}_u$, and $\boldsymbol{K}_e$, are adaptive. Starting with the concept of perfect model following, Kaufman et al.[13] derive an algorithm to compute the adaptive gains. The ideal model trajectories are considered to be reference target trajectories that the plant attempts to reach. The resulting adaptive controller can maintain small (bounded) tracking errors in nonideal environments and remains stable.

The adaptive algorithm to compute the input $\boldsymbol{u}_p$ to a linear time-invariant plant is summarized as follows. Let us define a vector $\boldsymbol{r}(t)$ that combines the three measurable signals and a matrix $\boldsymbol{K}_r(t)$ that concatenates the adaptive gains:

$$\boldsymbol{r}(t) = [\boldsymbol{e}_y(t), \boldsymbol{x}_m(t), \boldsymbol{u}_m(t)]^T, \qquad \boldsymbol{K}_r(t) = [\boldsymbol{K}_e(t), \boldsymbol{K}_x(t), \boldsymbol{K}_u(t)]$$

so that $\boldsymbol{u}_p$ can be written as

$$\boldsymbol{u}_p(t) = \boldsymbol{K}_r(t)\boldsymbol{r}(t) \tag{3}$$

To compute the adaptive gains, $\boldsymbol{K}_r$ is defined to be the sum of an integral and proportional component, that is,

$$\boldsymbol{K}_r(t) = \boldsymbol{K}_i(t) + \boldsymbol{K}_p(t) \tag{4}$$

with

$$\dot{\boldsymbol{K}}_i(t) = \boldsymbol{e}_y(t)\boldsymbol{r}^T(t)\boldsymbol{T}_i \tag{5}$$

$$\boldsymbol{K}_p(t) = \boldsymbol{e}_y(t)\boldsymbol{r}^T(t)\boldsymbol{T}_p \tag{6}$$

In Eqs. (5) and (6), the weighting matrices $\boldsymbol{T}_p$ and $\boldsymbol{T}_i$ are positive-definite symmetric and positive-semidefinite symmetric, respectively.

Note that the adaptive control algorithm cannot be applied to just any system. To guarantee that all states and gains in the adaptive system are bounded and the output error is asymptotically stable, it is necessary that the (linear, time-invariant) plant is almost strictly positive real (ASPR). This condition is based on the existence of an output feedback matrix, such that the ideal fictitious closed-loop system satisfies the positive-realness conditions required for stability of adaptive and other nonlinear controllers.[13] For nonlinear, time-varying systems, the similar concept of almost passivity is applicable. It is beyond the scope of this paper to discuss this here. In line with an example of the adaptive, longitudinal control for a relaxed static stability aircraft,[13] the adaptive system will be developed ad hoc and validated by computer simulation.

Thus far, an ideal environment has been considered. To cope with disturbances in an environment that lead to a persistent nonzero error and, therefore, to a continuous change in the integral gain $\boldsymbol{K}_i$, we will apply a robust design to adjust the integral gain to prevent it from reaching very high values. The integral term of Eq. (5) is adjusted in the following manner:

$$\dot{\boldsymbol{K}}_i = \boldsymbol{e}_y(t)\boldsymbol{r}^T(t)\boldsymbol{T}_i - \sigma_i\boldsymbol{K}_i(t) \tag{7}$$

Without the σ_i term, $\boldsymbol{K}_i(t)$ is a perfect integrator and may steadily increase (and even diverge) whenever perfect output following is not possible. Including the σ_i term, $\boldsymbol{K}_i(t)$ is obtained from a first-order filtering of $\boldsymbol{e}_y(t)\boldsymbol{r}^T(t)\boldsymbol{T}_i$ and, therefore, cannot diverge, unless the output error diverges.

IV. Control-System Design

A. Open-Loop Reference Model

A starting point in the development of the adaptive controller is the notion that the nonlinear space plane should behave like a stabilized, linear system for which the longitudinal and lateral motion are decoupled. Hence, as a reference model for the adaptive controller, a linearized model of the rotational dynamics is selected (the translational motion is assumed to have no influence on the rotational motion). At any point in the trajectory the reference model is supposed to be linearized around its trim equilibrium state. Summarized, the following equations hold:

$$\Delta\dot{p}_m = (1/I_{xx})\left(C_{l_\beta}\Delta\beta_m + C_{l_{\delta a}}\Delta\delta_{a,m} + C_{l_{\delta r}}\Delta\delta_{r,m}\right)q_{\mathrm{dyn}_e}S_{\mathrm{ref}}b_{\mathrm{ref}} \tag{8}$$

$$\Delta\dot{q}_m = (1/I_{yy})\left(C_{m_\alpha}\Delta\alpha_m + C_{m_{\delta e}}\Delta\delta_{e,m}\right)q_{\mathrm{dyn}_e}S_{\mathrm{ref}}c_{\mathrm{ref}} \tag{9}$$

$$\Delta\dot{r}_m = (1/I_{zz})\left(C_{n_\beta}\Delta\beta_m + C_{n_{\delta a}}\Delta\delta_{a,m} + C_{n_{\delta r}}\Delta\delta_{r,m}\right)q_{\mathrm{dyn}_e}S_{\mathrm{ref}}b_{\mathrm{ref}} \tag{10}$$

$$\Delta\dot{\sigma}_m = -\cos\alpha_e\Delta p_m - \sin\alpha_e\Delta r_m + [(g_e/V_e)\cos\gamma_e\cos\sigma_e - (L_e/mV_e)]\Delta\beta_m + (\tan\gamma_e/mV_e)\cos\sigma_e L_e\Delta\sigma_m \tag{11}$$

$$\Delta\dot{\alpha}_m = \Delta q_m - (1/mV_e)C_{L_\alpha}q_{\mathrm{dyn}_e}S_{\mathrm{ref}}\Delta\alpha_m \tag{12}$$

$$\Delta\dot{\beta}_m = \sin\alpha_e\Delta p_m - \cos\alpha_e\Delta r - (g_e/V_e)\cos\gamma_e\cos\sigma_e\Delta\sigma_m \tag{13}$$

In the preceding equations, Δ means that the equations are related to small deviations from the equilibrium state. The subscript m indicates that the variables are related to the reference model, whereas the subscript e stands for equilibrium value. Thus, in this case α_e and σ_e are identical to the guidance commands α_c and σ_c.

By defining a state vector $\boldsymbol{\Delta x}_m = (\Delta p_m, \Delta q_m, \Delta r_m, \Delta\alpha_m, \Delta\beta_m, \Delta\sigma_m)^T$ and a control vector $\boldsymbol{\Delta u}_m = (\Delta\delta_{a,m}, \Delta\delta_{e,m}\Delta\delta_{r,m})^T$, the preceding equations can be written in the state-space form of Eq. (2). The actual model state is the sum of the equilibrium and the perturbation values. As mentioned before, the equilibrium attitude is assumed to be equal to the commanded attitude issued from the guidance logic. The equilibrium (or commanded) angular rate is such that the derivatives of the aerodynamic angles α, β, and σ are zero. By defining an output vector $\boldsymbol{y}_m$, the reference model is completed with the output equation,

$$\boldsymbol{y}_m = \boldsymbol{x}_c + \boldsymbol{C}_m\boldsymbol{\Delta x}_m \tag{14}$$

such that

$$\boldsymbol{y}_m = (p_m, q_m, r_m, \sigma_m, \alpha_m, \beta_m)^T = (p_c + \Delta p_m, q_c + \Delta q_m, r_c + \Delta r_m, \sigma_c + \Delta\sigma_m, \alpha_c + \Delta\alpha_m, \Delta\beta_m)^T \tag{15}$$

Note that the control and output vectors of the plant, $\boldsymbol{u}_p$ and $\boldsymbol{y}_p$, are defined as

$$\boldsymbol{u}_p = (\delta_{a,p}, \delta_{e,p}, \delta_{r,p})^T, \qquad \boldsymbol{y}_p = (p_p, q_p, r_p, \sigma_p, \alpha_p, \beta_p)^T$$

To guarantee a stable reference model, a combination of an optimal proportional–integral (PI) controller for longitudinal motion and an analytic PD controller for lateral motion is included in the model.

The reference model is integrated in time to enable an update of the model state and control variables. A simple trapezoid rule that is usually applied to propagate a digital PID controller does not give a stable solution for the reference model. Therefore, the fixed-step fourth-order Runge–Kutta method is used, taking the sample time of the attitude controller as step size. Because the equilibrium state of the reference model is equal to the commanded state, the differential equations of the linearized model will yield zero derivatives once that equilibrium state is reached after an (initial) perturbation. In that case, the reference model state is represented by the commanded attitude and angular rates, and the control variables are given by the trimmed deflection angles. This would even make the reference model superfluous.

However, if there is an abrupt change in the commanded attitude, the response of the model to this change and the corresponding perturbation control should be used as much as possible to shape the nonlinear vehicle control vector. For this reason, we take the difference in guidance commands of two successive samples and excite the reference model with a step corresponding with this difference. In the consecutive sample the model controller will try to bring back the model to its equilibrium state, thereby generating perturbation-control commands. Note that the initial state of the model will be put equal to that of the nonlinear vehicle. In this way, any abrupt reaction of the vehicle will be minimized. In the remainder of this section, the reference-model controller will be discussed.

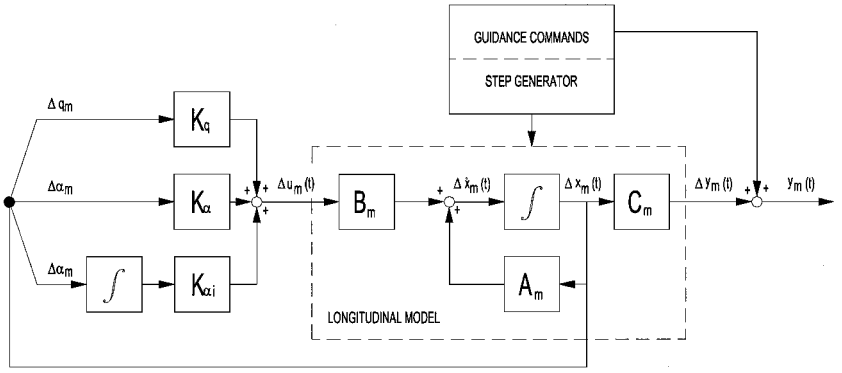

Fig. 1 Closed-loop reference model for longitudinal motion.

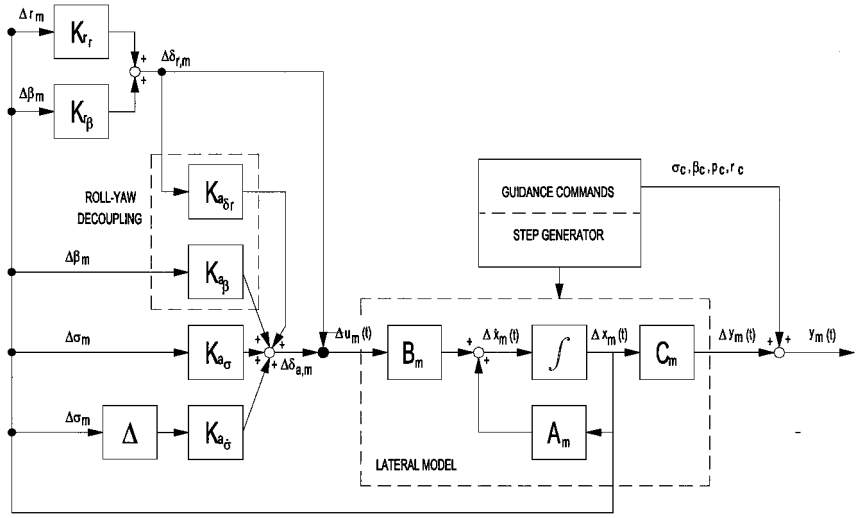

Fig. 2 Closed-loop reference model for lateral motion.

B. Reference-Model Controller

The longitudinal control law is defined as (Fig. 1)

$$\Delta\delta_{e,m} = K_{e_q}\Delta q_m + K_{e_\alpha}\Delta\alpha_m + K_{e_{\int\alpha}}\int_0^t \Delta\alpha_m \,\mathrm{d}t \qquad (16)$$

The preceding control law can be interpreted as a PID control law for α because the inclusion of q provides physical damping. The integral component has been added to reduce the steady-state error in α to zero because the performance of the propulsion system is dependent on, amongst others, α. The gain matrix is calculated by minimizing a quadratic cost criterion on an indefinite control time interval,[19] making this controller a linear quadratic regulator.

The lateral controller operates the rudder to control the yaw motion and the ailerons to control the roll motion (Fig. 2). The contribution of the ailerons to the yaw moment is neglected, and it is assumed that the space plane is flying at small α. The rudder control law is given by

$$\Delta\delta_{r,m} = K_{r_r}\Delta r_m + K_{r_\beta}\Delta\beta_m \qquad (17)$$

where the gains are obtained analytically by deriving the characteristic equation for yaw motion and writing it as a second-order transfer function, defined by a damping factor $\zeta_{r,m}$ and eigenfrequency $\omega_{r,m}$. This yields[16,18]

$$K_{r_r} = -2\left(I_{zz}\big/N_{\delta_r}\right)\zeta_{r,m}\omega_{r,m}, \qquad K_{r_\beta} = \left(I_{zz}\big/N_{\delta_r}\right)\omega_{r,m}^2 - \left(N_\beta\big/N_{\delta_r}\right) \qquad (18)$$

In the preceding expressions for the gains, N_β and N_{δ_r} are the yaw-moment derivatives with respect to β and δ_r, respectively.

The bank controller drives the ailerons to achieve the commanded bank angle issued by the guidance system with the following aileron-control law, which follows after inspecting Eqs. (8) and (11):

$$\Delta\delta_{a,m} = K_{a\beta}\Delta\beta_m + K_{a_{\delta_r}}\Delta\delta_{r,m} + K_{a_\sigma}\Delta\sigma_m + K_{a_{\dot\sigma}}\Delta\dot\sigma_m \qquad (19)$$

To decouple the roll and yaw motion, it is necessary to eliminate the first two terms of the right-hand side of Eq. (19). When Eq. (19) is substituted into Eq. (8), the required gains for roll–yaw decoupling are found to be

$$K_{a\beta} = -\left(L_\beta\big/L_{\delta_a}\right), \qquad K_{a_{\delta_r}} = -\left(L_{\delta_r}\big/L_{\delta_a}\right) \qquad (20)$$

where L_β, L_{δ_a}, and L_{δ_r} are the roll-moment derivatives with respect to β, δ_a, and δ_r, respectively. The remaining two gains can be expressed as a function of the characteristic values of a second-order transfer function, $\zeta_{p,m}$ and $\omega_{p,m}$ (Ref. 16):

$$K_{a_{\dot\sigma}} = \left(I_{xx}\big/L_{\delta_a}\right)\left[(\tan\gamma_e/mV_e)\cos\sigma_e L_e + 2\zeta_{p,m}\omega_{p,m}\right]$$
$$K_{a_\sigma} = \left(I_{xx}\big/L_{\delta_a}\right)\omega_{p,m}^2 \qquad (21)$$

C. Total-System Model

To apply MRAC, the reference model (6 states for attitude and angular rates) and the nonlinear WCC (12 states for position, velocity, attitude, and angular rates) have to be combined into one dynamic simulation model (Fig. 3). Moreover, the reference-model controller parameters and the parameters that are required to compute the adaptive gains must be specified. To begin with the reference model, the maximum state deviation and control effort to compute the gains for the longitudinal controller given by Eq. (16) are chosen to be

$$\Delta q_{m,\max} = 0.5 \text{ deg/s}, \qquad \Delta\alpha_{m,\max} = 0.2 \text{ deg}$$

$$\left[\int \Delta\alpha_m \,\mathrm{d}t\right]_{\max} = 0.1 \text{ deg/s}, \qquad \Delta\delta_{e_m,\max} = 20 \text{ deg}$$

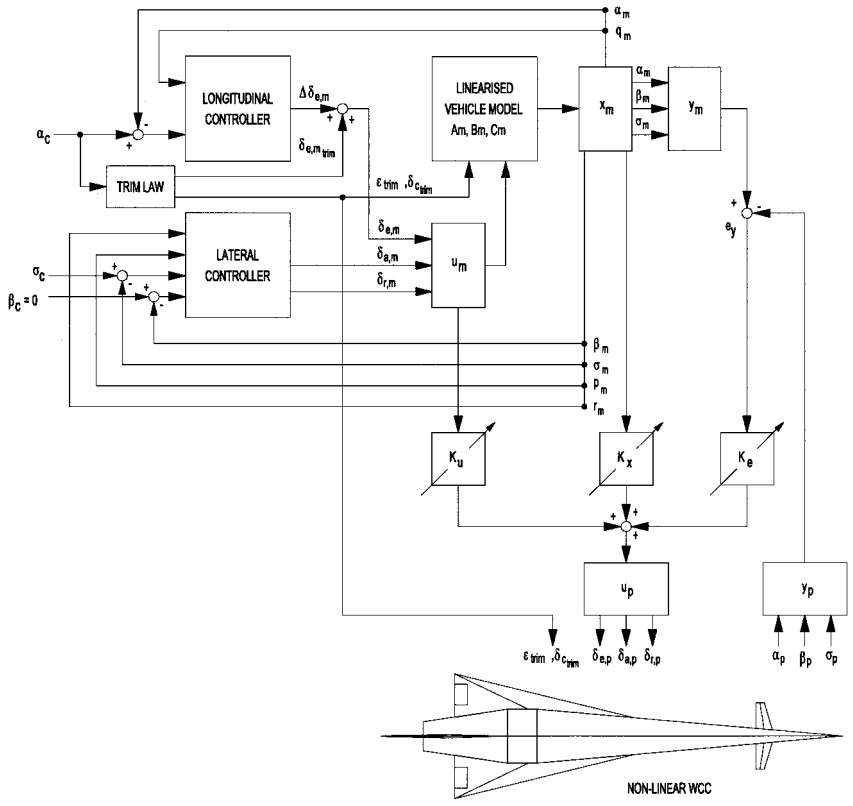

Fig. 3 Integrated MRAC system.

For the lateral controller, the values of Ref. 18 are used, where a similar controller has been applied directly to the nonlinear model of the WCC, that is,

$$\zeta_{p,m} = \zeta_{r,m} = 0.707, \qquad \omega_{p,m} = \omega_{r,m} = 3.0 \text{ rad/s}$$

With respect to the output error $\boldsymbol{e}_y$, some remarks must be made. In the initial design only the aerodynamic angles were part of the model and plant output vector, thus defining $\boldsymbol{e}_y$ as the difference between the two. It appeared to be very difficult to get a stable controller while using only the basic MRAC system. The stability can be improved in a mathematical manner, that is, by adding feedforward compensators around the plant and the model, or, more generally, by including supplementary dynamics in cascade, parallel, or feedback with the plant.[13]

However, the stability can also be improved in a more or less physical manner, by using more information of the rotational motion of both model and plant, which is found back in the error derivative. The error derivative (or, similarly, the angular rate) can serve as a measure of the damping, for example, a rather large difference implies that the vehicle is changing its attitude too fast as compared with the model, and it would, therefore, be better if the deflection angles are restrained to avoid overshoot and possible oscillations.

Because the output error can only have as many elements as the number of controls, each of the attitude errors is blended with its derivative to form $\boldsymbol{e}_y$:

$$\boldsymbol{e}_y = \begin{pmatrix} \sigma_{\text{err}} + k_{e\dot{\sigma}}\dot{\sigma}_{\text{err}} \\ \alpha_{\text{err}} + k_{e\dot{\alpha}}\dot{\alpha}_{\text{err}} \\ \beta_{\text{err}} + k_{e\dot{\beta}}\dot{\beta}_{\text{err}} \end{pmatrix} \tag{22}$$

The error-derivative gains $k_{e\dot{\sigma}}$, $k_{e\dot{\alpha}}$, and $k_{e\dot{\beta}}$ can be found by doing some response tests. Values between 0.05 and 0.1 are found to yield satisfactory results.

The weighting matrices $\boldsymbol{T}_p$ and $\boldsymbol{T}_i$ are 12×12 matrices and, if completely defined, represent a total of 288 weighting coefficients. However, it is common practice for a first design to define only the diagonal elements,[13] thereby reducing the number of coefficients to 24. Furthermore, 12 integral-gain coefficients $\sigma_{i,j}\,(j = 1, \ldots, 12)$, representing each of the elements of the concatenated vector $\boldsymbol{r}$, can be selected to increase the robustness of the controller in the presence of persistent steady-state errors. The numerical values of the controller parameters are usually found by trial and error, based on the experience of the designer. Careful selection of the parameters and analysis of the response will finally lead to an adequate performance of the adaptive controller. Application of a numerical optimization technique,[12] or, alternatively, a response-surface methodology,[20] to determine (sub-)optimal values of the controller parameters is beyond the scope of the current study. Note, it was necessary to increase the sample rate of the controller to a frequency of 200 Hz for an acceptable response. It may be possible that the sample rate can be decreased once optimal weighting factors have been found.

Table 1 MRAC parameter values for the $M = 5.6$ flight condition

Roll		Pitch		Yaw	
Parameter	Value	Parameter	Value	Parameter	Value
$T_{p,\sigma_{\text{err}}}$	3,000	$T_{p,\alpha_{\text{err}}}$	8,000	$T_{p,\sigma_{\text{err}}}$	6,000
$T_{i,\sigma_{\text{err}}}$	10,000	$T_{i,\alpha_{\text{err}}}$	8,000	$T_{i,\sigma_{\text{err}}}$	100
$T_{p,\beta_{\text{err}}}$	5,000	T_{p,q_m}	200	$T_{p,\beta_{\text{err}}}$	10,000
$T_{i,\beta_{\text{err}}}$	100	T_{i,q_m}	50	$T_{i,\beta_{\text{err}}}$	10,000
T_{p,p_m}	100	T_{p,α_m}	800	T_{p,r_m}	200
T_{i,p_m}	50	T_{i,α_m}	100	T_{i,r_m}	50
T_{p,σ_m}	600	$T_{p,\delta_{e,m}}$	30	T_{p,β_m}	800
T_{i,σ_m}	100	$T_{i,\delta_{e,m}}$	50	T_{i,β_m}	100
$T_{p,\delta_{a,m}}$	600	$\sigma_{i,\alpha}$	0.2	$T_{p,\delta_{r,m}}$	600
$T_{i,\delta_{a,m}}$	50	——	——	$T_{i,\delta_{r,m}}$	50
$\sigma_{i,\sigma}$	0.2	——	——	$\sigma_{i,\beta}$	0.2

The values for the MRAC weighting coefficients are listed in Table 1. Some remarks should be made. First, the parameter values are chosen such that an acceptable response is guaranteed, without trying to optimize this response. We also found that for other flight conditions (higher or lower Mach numbers), different parameter values would improve the response. A future extension could be

weighting coefficients as a function of Mach number. Second, only nonzero diagonal elements for $\boldsymbol{T}_p$ and $\boldsymbol{T}_i$ are defined. Off-diagonal elements are all zero. Third, we distinguish three sets of coefficients for each of the three rotations roll, pitch, and yaw. Kaufman et al.[13] do not discuss this because they only consider single-input/single-output systems. However, we found that if the weighting coefficient of, for instance, α_{err} is large (which is required for an adequate pitch response) and large errors in both α and β are occurring simultaneously, then the contribution to the rudder deflection is also large, and in our case it appeared to be too large. For that reason, a small weighting coefficient for α_{err} would be favorable, but this would give a slow pitch response. This was solved by defining the weighting coefficients for each of the three controls independently. The remaining coefficients that are not listed in each of the columns are defined to be 10^{-6} for the proportional gains (to meet with the positive definiteness of $\boldsymbol{T}_p$) and 0 for the integral gains (to meet with the positive semidefiniteness of $\boldsymbol{T}_i$). Fourth, the integral-gain coefficients are the same for each of the integral gains.

V. Simulation Results

A. Evaluation

In this subsection, some aspects that came forward while designing the MRAC system, both for the fundamental response tests discussed in this paper and the vertical-plane ascent to orbit,[16] will be evaluated. As was mentioned before, initially $\boldsymbol{e}_y$ was based on only the aerodynamic angles α, β, and σ. Most of the encountered instabilities were found with the application of this output error, pointing at the low damping that the controller could provide in case only the basic MRAC algorithm is applied. Increasing the damping by including the angular-rate error in the output error improved the results considerably, even completely removing some of the instabilities. However, because the gained experience is worth sharing, it will briefly be discussed.

In the process of designing the adaptive controller, it was found that discontinuities in the aerodynamic coefficients (due to the applied linear interpolation) can cause instabilities when the weighting factors are not large enough. The first discontinuity was found when the elevon deflection changed sign. The left derivative (negative deflection angles) is smaller than the right one (positive deflections). This means that when the elevon trim deflection is negative (but close to zero) and the corrective elevon deflection is such that the total elevon deflection is slightly positive, the larger right derivative causes a too large pitch moment that induces an oscillation in pitch. This oscillation could be controlled by increasing the proportional gains. However, an adjustment of the interpolation scheme that is used to compute the elevon trim deflection angle such that continuous derivatives are obtained is advisable. One can think of cubic spline interpolation that is also commonly used in trajectory optimization. A similar problem occurred while reaching the Mach 6 flight condition, another node in the aerodynamic tables. Also in this case, the left and right derivatives are different. Note that the attitude controller should, of course, be that robust that it can easily handle these discretizations, as is, in fact, the case with the blended output error.

The adaptive controller requires relatively large weighting factors, especially for the integral gains, if accurate α control is pursued. Thus, the integral gains become large, and when sudden α_c changes are commanded, oscillations can be induced due to the large commands. This can be prevented if the integral gains are reset (or largely reduced) before the α_c command takes place. However, it should be studied how this can be done in a smooth manner, similarly to the σ_i compensation. Note that a large value of σ_i reduces the integral gain but also decreases the efficiency of integral control.

Because of the large weighting factors, sudden changes in commanded attitude result in large deflections, basically due to the inertia of the vehicle and, therefore, increasing attitude errors. This can lead to oscillations in, for instance, the angle of attack and, thus, the flight-path angle. One way to improve the damping of the pitch control, apart from using the blended output error, might be to use nonzero entries for the off-diagonal elements of the weighting matrix. It remains to be studied in what way the response of the system can be affected, although it has been found elsewhere that the results can be positively influenced.[12,20]

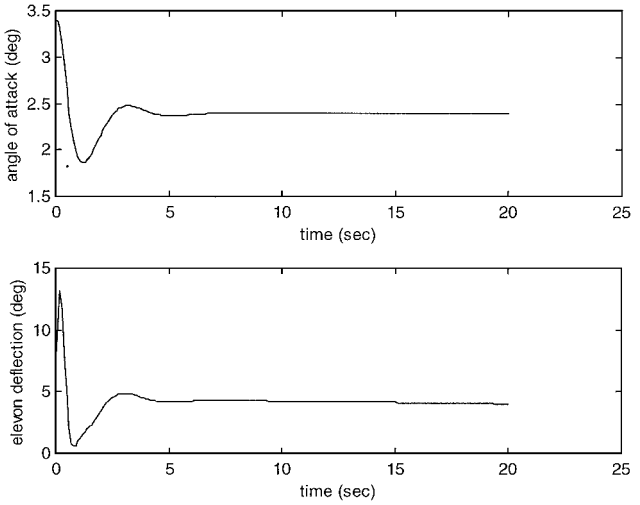

Fig. 4 Angle of attack (top) and elevon deflection (bottom) vs time after an initial disturbance $\Delta\alpha$ = 1 deg.

For the nominal ascent mission, it appeared that the guidance commands could serve as a reference model. This is because the attitude controller included in the reference model is relatively fast, that is, it can track the guidance commands almost instantaneously. This means that the reference state is almost equal to the guidance commands. Because the main contribution to the elevator command is the trim angle, the corrective control coming from the reference model is practically zero. In fact, the nonlinear space plane is, in principle, behaving like the linear reference model. Note that, for lateral motion, the nominal aileron and rudder deflections are zero, such that the corrective control can have an impact on the definition of the plant control vector, especially when the corrective control is large, for example, during hypersonic turns.

Unfortunately, also discrete changes in α_c are immediately followed, and this results in some oscillatory behavior of the WCC, as will be discussed later. It is, therefore, recommended that designing the reference model including attitude controller should not be regarded lightly. The response of the reference model to the guidance commands should be smooth, especially at those flight conditions where the aerodynamic forces and moments are large. It should also be understood that continuous guidance commands without abrupt changes will enhance the performance of the MRAC system when applied in supersonic and hypersonic flight.

Concluding this subsection, we will briefly discuss the results of a flight at constant $\alpha = 2.4$ deg ($M = 5.6$). In one case, the initial α is perturbed with $\Delta\alpha = 1$ deg, and in a second case $\Delta\sigma = 5$ deg is added to the initial σ. In Fig. 4, α_{err} is plotted as well as the corresponding total elevon deflection, that is, trim value plus corrective control. It is clear that because of a large initial elevon deflection ($\Delta\delta_e \approx 9$ deg), a fast response is obtained, though as a result there is an overshoot in α of almost 0.6 deg. The angle of attack stabilizes at 2.4 deg after about 8 s. A disadvantage may be that for larger α_{err} the elevons get saturated.

A similar bank-angle response is observed when σ_0 is perturbed with $\Delta\sigma = 5$ deg. The initial response is fast (Fig. 5) whereas the overshoot is about 0.5 deg. The aileron deflection, though, is smaller than $\Delta\delta_e$, that is, $\Delta\delta_a \approx 4.5$ deg, which is due to a lower inertia about the X_B axis. The augmented roll damping is lower than the augmented pitch damping, which shows a somewhat stronger oscillatory behavior, although the amplitude is quite small. A small induced β is observed ($\Delta\beta \approx 0.15$ deg), which indicates that although the roll–yaw motion is not completely decoupled the coupling is not so strong. The coupling can probably even be further reduced by optimizing the controller. The rudder deflection is only 0.2 deg.

In conclusion, the first results obtained by using the MRAC system are promising and form the basis for a more detailed evaluation.

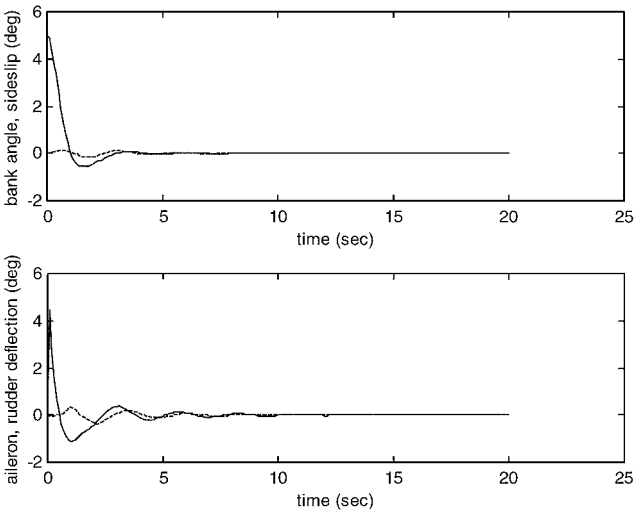

Fig. 5 Bank-angle (——) and side-slip error (- - -) vs time (top) and corresponding aileron (——) and rudder (- - -) deflection after an initial disturbance $\Delta\sigma$ = 5 deg.

B. Altitude Transition

To reach a target orbit with nonzero inclination, the final ascent is started at a latitude equal to the orbit inclination. When the latitude of the launch base is not equal to the target latitude, a cruise flight may be necessary before the pull up that marks the beginning of the final ascent. In this subsection, an altitude transition (step command of $\Delta h_c = 1000$ m) and subsequent cruise flight at a maximum dynamic pressure of 95,000 N/m^2 will be studied for $M = 5.6$. The following nonzero initial conditions hold for a flight along the equator: $V_0 = 1667.0$ m/s, $h_0 = 21{,}641$ m, $m_0 = 118{,}968$ kg, $\delta_{T0} = 0.2$, and $\alpha_0 = 2.8$ deg.

The values for the MRAC weighting coefficients are listed in Table 1. Moreover, limitations are considered on α_c ($\alpha_{c,\min} = 2.4$ deg and $\alpha_{c,\max} = 3.2$ deg) and δ_T ($\delta_{T,\min} = 0.1$ and $\delta_{T,\max} = 0.5$). Also the influence of a steady-state wind will be studied. The wind model is based on the GRAM-95 model,[21] which, although it has been defined for NASA Kennedy Space Center, is representative for most winds at such an altitude. The wind vector is defined as a number of discrete east–west zonal components as a function of altitude: $V_w = 12.2$ m/s($h = 20.0$ km), 10.4 m/s (21.0 km), 10.0 m/s (22.0 km), 10.2 m/s (23.0 km), and 10.6 m/s (24.0 km). Linear interpolation is used to obtain intermediate values.

In Fig. 6, h is plotted as a function t. It can clearly be seen that the altitude transition is smooth and the space plane takes about 150 s to reach a stable cruise-flight condition. The influence of the steady-state wind shows as a delay in the ascending flight. Because the WCC is flying against the wind, q_{dyn} is increased and δ_T will be decreased. This results in a lower ground velocity and, hence, a longer climb. From Fig. 6, it is obvious that δ_T is oscillating to account for the head wind and to lower q_{dyn}. However, because of the relative fast response and the limit on δ_T (10%/s), it takes awhile before a stable condition is reached. A review of the throttle-control law should prevent these kind of oscillations (note, q_{dyn} could be kept at 95 kPa once equilibrium was reached). Finally, the shift in the two throttle curves corresponds with the shift in the two height curves.

Figure 7 shows α_{err} and δ_e as a function of time. The largest deviations from α_c occur at the beginning of the climb ($t = 0$ s) and at the end of the climb ($t \approx 90$ s), when the guidance system commands a smaller α to decrease the climb rate. For the no-wind case, the error is well damped, and, in general, the control error is very small. In case there is wind, there are some larger errors up to $t \approx 40$ s, corresponding with the oscillating δ_T. Any sharp peak in δ_e corresponds with a peak value in α_{err} and aims at reducing this control error. Note that σ and β were not affected by this maneuver and remained zero throughout the flight.

In conclusion, the attitude controller is capable of following guidance commands for an altitude transition and remains stable during the subsequent cruise flight. The presence of a steady-state wind does not seem to influence the performance of the attitude controller.

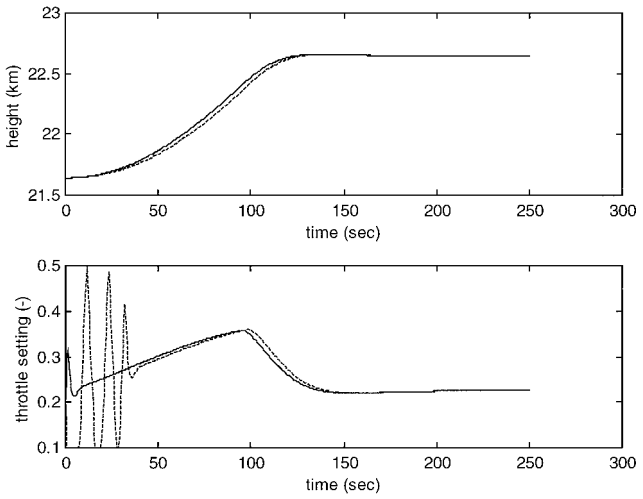

Fig. 6 Height vs time (top) for Δh_c = 1000 m without (——) and with (- - -) wind, as well as the corresponding throttle setting.

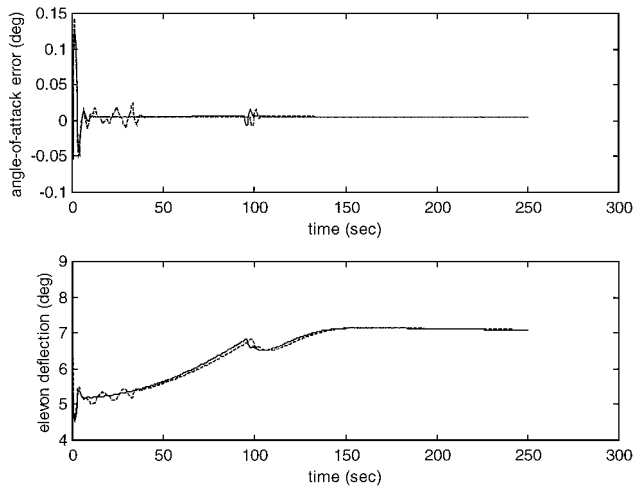

Fig. 7 Angle-of-attack error vs time for Δh_c = 1000 m without (——) and with (- - -) wind, including elevon deflection (bottom).

C. Cross-Range Transition

Starting from the same initial conditions as in the preceding subsection, a cross-range transition of 2000 m is simulated. This maneuver consists of a small initial heading change toward the south and a correcting change to bring the heading back to due east. A positive cross-range transition results in this case in a target latitude south of the equator.

In Fig. 8, the cross-range and altitude error have been plotted as a function of time. The initial error in Δy is, of course, equal to the commanded 2000 m. We see a smooth decrease and in the no-wind case a rather large overshoot. It appeared that the PID controller that is applied in the cross-range guidance is very sensitive to the integral gain. A very small gain value will decrease the overshoot but will also significantly increase the response time. Because the PID gain values were established by trial and error, it is expected that the performance will be improved once the closed-loop system is properly analyzed. It is remarkable to see that the presence of a head wind acts to stabilize in the sense that the overshoot is smaller and equilibrium is reached must faster, although it takes somewhat longer to cover the 2000 m. The explanation can be found in the altitude-error history. This error is larger in case there is wind. Because altitude control has priority over cross-range control, and the commanded load factor is close or even equal to its maximum allowable value, there is only limited or no cross-range control (which has been verified by inspecting σ_c). This means that once cross-range control is started again, the vehicle has already covered a significant part of the 2000 m and can suffice with a smaller σ_c, which results in the smaller overshoot.

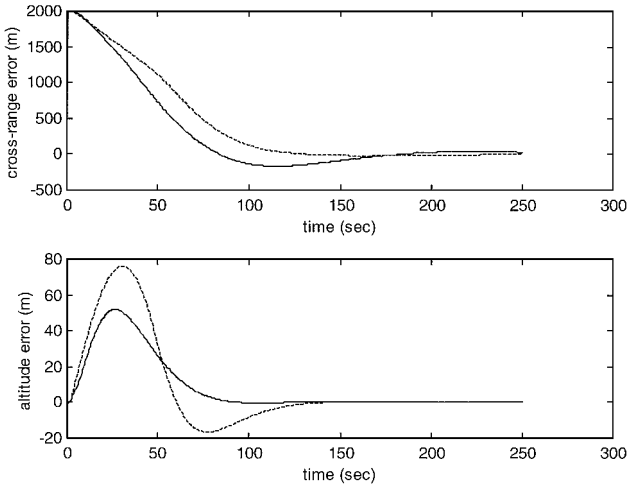

Fig. 8 Cross-range error vs time for Δy_c = 2000 m without (——) and with (– – –) wind, as well as corresponding altitude error (bottom).

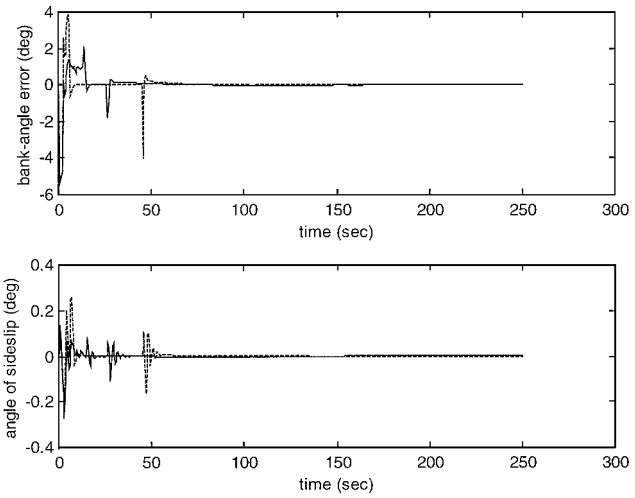

Fig. 9 Bank-angle error (top) and angle of side slip (bottom) vs time for Δy_c = 2000 m without (——) and with (– – –) wind.

Part of this reasoning is confirmed by Fig. 9. The bank-angle error becomes zero after the first 10 s of flight, and the next command shows as a peak in σ_{err} at $t \approx 45$ s. The initial σ_c is large, that is, −22 deg, which explains the large control error. However, the attitude controller is stable and quickly reduces the error to zero. Figure 9 also shows the induced β, caused by the roll–yaw coupling. The MRAC system is apparently not capable of uncoupling the roll and yaw motion. Further study on how the weighting coefficients need to be altered to accomplish this is required.

The elevon and rudder deflections basically give similar peaks as the corresponding control errors. Only during the first 50 s there is some strong activity, mainly due to the aileron function to initiate the roll maneuver for tilting the lift force and, hence, to start the cross-range transition. The rudder deflection is basically very small ($\approx \pm 1.2$ deg). Indeed, it is possible to deflect the rudder at larger angles to minimize the induced β.

In conclusion, although it seems that the attitude controller is capable of following σ_c and to minimizing the induced β during a cross-range transition, it seems that the performance should be further improved before it can be called robust.

D. Sensitivity Analysis

For the sensitivity analysis, a combined altitude and cross-range transition of 1000 m each will be considered. Initial conditions and MRAC weighting coefficients are the same as before.

Analysis of the results will focus on the performance of the control system. The selected responses are the maximum control errors α_{err}, β_{err}, and σ_{err}, and the control-surface activity that is given by the mean and standard deviation of the deflection angles. The six factors that we include are the following: $\Delta X_{cm} = \Delta Y_{cm} = \Delta Z_{cm} = \pm 0.1$ m and $\Delta C_l = \Delta C_m = \Delta C_n = \pm 5\%$, and they will be varied according using a design-of-experiments approach.[22] The factors are (arbitrarily) assigned to the leftmost columns of the two-level L_8 orthogonal array. Note that we will not try to establish the existence of particular interactions.

Executing the simulations shows that four out of the eight runs end in unstable oscillations (runs, 2, 4, 5, and 8). Run 2 even resulted in a crash of the vehicle. Part of the explanation can be found in the design of the guidance system. Initially, a cross-range command is generated that results in a small heading change. However, the moment the load limits are reached, priority is given to altitude control. Because in the presence of the disturbances it is not quite possible to reduce the altitude error to zero, the guidance system does not issue a commanded bank angle differing from zero for a long time. In the mean time, the covered cross range increases due to a heading that deviates from the initial heading. The moment the load limit is relaxed, the guidance system is faced with a large cross-range error, and the subsequent σ_c in combination with the perturbations is, in some cases, the cause of unstable oscillations.

In trying to understand to what extent the guidance system is at fault and to what extent fault lies with the attitude controller, as an example we will analyze one of the trajectories that does not exhibit attitude oscillations (run 1). In Fig. 10 the altitude error is shown (the cross-range error is steadily increasing, due to a fixed heading and load limits that prevent active cross-range guidance). It is clear that the guidance system is not capable of reducing both errors to zero. The altitude error exhibits an oscillatory behavior that even seems to diverge at the end of the simulation interval. Because of a change in altitude and velocity, δ_T is varying significantly to keep tracking the dynamic-pressure constraint.

A question arises now: Is the attitude controller responsible for the guidance errors? In Fig. 11 the control errors in α, σ, and β are depicted. The solid line represents α_{err} and is quite close to zero, although the error is slowly diverging and reaches a final value of just over 0.15 deg. This means that the attitude controller is capable of following α_c. The long-dashed line shows σ_{err}. Apart from two peak values of about −4 and −1 deg when the only two major cross-range guidance commands are issued, the error has a constant bias of about −0.2 deg. Although the attitude controller cannot reduce this error to zero in the presence of the perturbations, the error remains bounded (and small). The third curve (dash–dot) is difficult to distinguish: β is practically zero. A maximum (absolute) value of 0.2 deg was found at $t \approx 45$ s. From the corresponding corrective elevator and aileron deflections, it is obvious that due to the perturbations a nonzero equilibrium value for both is required. Once the nonzero aileron defection is added to the trimmed elevon deflection, an asymmetric deflection of the left and right elevon is the result with a difference of about 2 deg.

In conclusion, at least for the results of this single run, the attitude controller seems to be performing reasonably well. Apparently, the

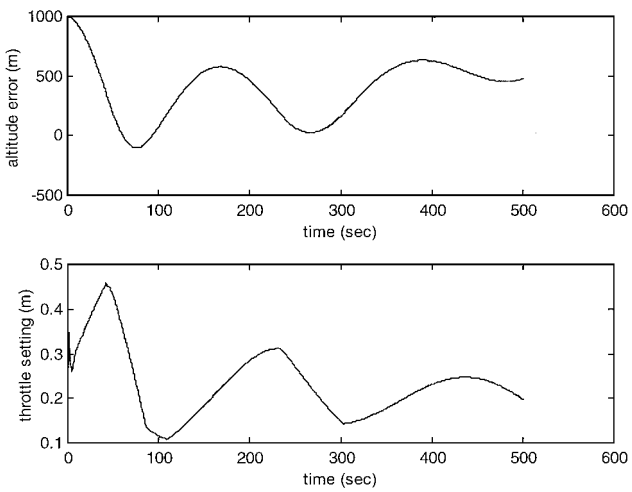

Fig. 10 Altitude error (top) and throttle setting (bottom) vs time for run 1 of the sensitivity analysis.

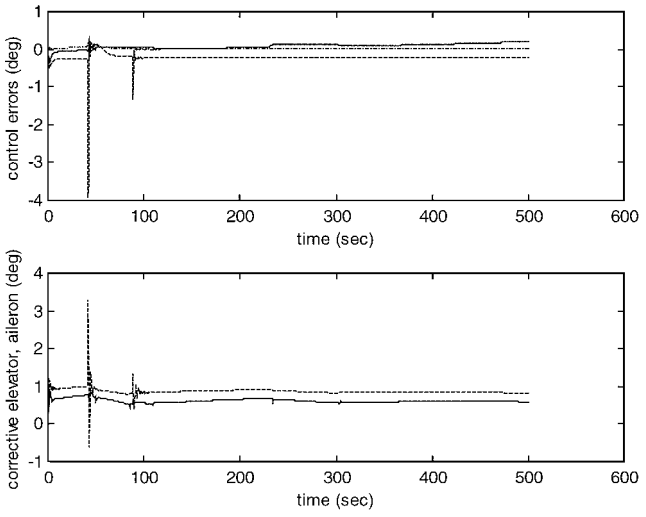

Fig. 11 Control errors in α (——), σ (- - -), and β (- - - -) for run 1 of the sensitivity analysis (top), including the corrective elevator (——) and aileron (- - -) vs time (bottom).

guidance system cannot adequately reduce the altitude and cross-range error and should be carefully reviewed.

VI. Conclusions

The fundamental design of an MRAC control system is relatively easy. Unfortunately, there are many design parameters that have to be defined by the designer, and unless the designer's experience is extensive this can be very time consuming. An alternative would be to define performance parameters for the attitude controller, such as integrated control errors and deflection angles, and maximum allowable values of these parameters. An optimization process can then be carried out to determine the weighting coefficients, but because this number can be quite large, it remains a complicated matter. In this study, we have applied the basic MRAC algorithm and defined the weighting coefficients by trial and error. Only the diagonal elements have been used, and it remains to be studied how off-diagonal elements can influence the performance. The damping of the system has been improved by blending the output error with its derivative.

Some aspects that came forward during the design process of the MRAC system include that discontinuities in the aerodynamic coefficients can cause instabilities when the weighting factors are not large enough. When the integral gains can increase to large values, a strong response can be expected when there are discontinuities in the input signal. This effect can be reduced by including so-called integral coefficients σ_i, although a large value of σ_i decreases the efficiency of integral control. Combination of roll, pitch, and yaw control in one MRAC control system, and the application of one set of weighting matrices, can give rise to conflicting demands when simultaneously large output errors occur. In this study, this is solved by defining three different sets of weighting matrices.

Applying the MRAC system to nominal hypersonic maneuvers showed that the controller is capable of following the guidance commands for an altitude and cross-range transition and that it can remain stable during the subsequent cruise flight. The presence of a steady-state wind does not seem to influence the performance. However, considering lateral control, it seems that the performance should be further improved before the controller can be called robust. During the succeeding sensitivity analysis, the limitations of the guidance system were revealed, where the attitude controller has a reasonable performance for at least a number of simulations. A point of attention is the relatively high sample rate of the controller that may be reduced once the weighting matrices have been optimized.

The next step in the research is to further improve the performance of the adaptive controller by optimizing the weighting factors and/or by including feedforward compensators around the plant and/or reference model. Once the rigid-body motion can be properly controlled, (i.e., the controller is robust), the next step will be the inclusion of aeroelasticity and turbulence models, as well as a gradual expansion of the flight envelope, that is, ranging from zero to orbital velocity.

References

[1]Maus, J. R., Griffith, B. J., and Szema, K. Y., "Hypersonic Mach Number and Real Gas Effects on Space Shuttle Orbiter Aerodynamics," *Journal of Spacecraft and Rockets*, Vol. 21, No. 2, 1984, pp. 136–141.

[2]Schmidt, D. K., Mamich, H., and Chavez, F., "Dynamics and Control of Hypersonic Vehicles—the Integration Challenge for the 1990s," AIAA Paper 91-5057, Dec. 1991.

[3]Raney, D. L., McMinn, J. D., and Pototzky, A. S., "Impact of Aeroelastic–Propulsive Interactions on Flight Dynamics of a Hypersonic Vehicle," *Journal of Aircraft*, Vol. 32, No. 2, 1995, pp. 355–362.

[4]McRuer, D., "Design and Modelling Issues for Integrated Airframe/Propulsion Control of Hypersonic Flight Vehicles," *Proceedings of the American Control Conference*, 1991, pp. 729–735.

[5]Schwanz, R. C., and Cerra, J. J., "Dynamic Modelling Uncertainty Affecting Control System Design," AIAA Paper 84-1057, May 1984.

[6]Buschek, H., and Calise, A. J., "Robust Control of Hypersonic Vehicles Considering Propulsive and Aeroelastic Effects," AIAA Paper 93-3762, Aug. 1993.

[7]Gregory, I. M., Chowdhry, R. S., McMinn, J. D., and Shaughnessy, J. D., "Hypersonic Vehicle Model Control Law Development Using H_∞ and μ-Synthesis," NASA TM-4562, 1994.

[8]Grocott, S. C. O., How, J. P., and Miller, D. W., "Comparison of Robust Control Techniques for Uncertain Structural Systems," AIAA Paper 94-3571, 1994.

[9]Vincent, J. H., Emami-Naeini, A., and Khraishi, N. M., "Case Study Comparison of Linear Quadratic Regulator and H_∞ Control Synthesis," *Journal of Guidance, Control, and Dynamics*, Vol. 17, No. 5, 1994, pp. 958–965.

[10]Boskovich, B., and Kaufmann, R. E., "Evolution of the Honeywell First-Generation Adaptive Autopilot and its Applications to F-94, F-101, X-15, and X-20 Vehicles," *Journal of Aircraft*, Vol. 3, No. 4, 1966, pp. 296–304.

[11]Landau, I., "A Survey of Model Reference Adaptive Techniques: Theory and Applications," *Automatica*, Vol. 10, 1974, pp. 353–379.

[12]Messer, R. S., Haftka, R. T., and Cudney, H. H., "Cost of Model Reference Adaptive Control: Analysis, Experiments, and Optimization," *Journal of Guidance, Control, and Dynamics*, Vol. 17, No. 5, 1994, pp. 975–982.

[13]Kaufman, H., Bar-Kana, I., and Sobel, K., *Direct Adaptive Control Algorithms*, Springer-Verlag, New York, 1994.

[14]Ih, C.-H. C., Wang, S. J., and Leondes, C. T., "Adaptive Control for the Space Station," *IEEE Control Systems Magazine*, 1987, pp. 29–34.

[15]Bar-Kana, I., and Kaufman, H., "Simple Adaptive Control of Large Flexible Space Structures," *IEEE Aerospace and Electronic Systems Magazine*, Vol. 29, No. 4, 1993, pp. 1137–1149.

[16]Mooij, E., "Aerospace-Plane Flight Dynamics: Analysis of Guidance and Control Concepts," Ph.D. Dissertation, Faculty of Aerospace Engineering, Delft Univ. of Technology, Delft, The Netherlands, 1998.

[17]Shaughnessy, J. D., Zane-Pinckney, S., McMinn, J. D., Cruz, C. I., and Kelley, M. L., "Hypersonic Vehicle Simulation Model: Winged-Cone Configuration," NASA TM 102610, Nov. 1990.

[18]Raney, D., and Lallman, F., "Control Integration Concept for Hypersonic Cruise-Turn Maneuvers," NASA TP 3136, 1992.

[19]Gopal, M., *Modern Control System Theory*, 2nd reprint, Wiley Eastern, New Delhi, India, 1989, Chap. 11.

[20]Mooij, E., " Direct Model Reference Adaptive Control of a Winged Reentry Vehicle," AIAA Paper 99-4834, Nov. 1999.

[21]Justus, C. G., Jeffries, W. R., III, Yung, S. P., and Johnson, D. L., "The NASA/MSFC Global Reference Atmospheric Model—1995 Version (GRAM-95)," NASA TM 4715, 1995.

[22]Taguchi, G., *System of Experimental Design. Engineering Methods to Optimize Quality and Minimize Costs*, Vol. 1, 2nd printing, UNIPUB/Kraus International, White Plains, NY, 1988.